Combining a glycolysis-related prognostic model based on scRNA-Seq with experimental verification identifies ZFP41 as a potential prognostic biomarker for HCC

YU TENG[1,2], JIANRONG XU[2], YAOQUN WANG[2,3], NINGYUAN WEN[2,3], HUI YE[2,3] and BEI LI[2,3]

[1]West China School of Medicine, Sichuan University; [2]Research Center for Biliary Diseases; [3]Division of Biliary Tract Surgery, Department of General Surgery, West China Hospital, Sichuan University, Chengdu, Sichuan 610041, P.R. China

Received October 23, 2023; Accepted February 27, 2024

DOI: 10.3892/mmr.2024.13203

Abstract. Hepatocellular carcinoma (HCC) is a common malignancy with a poor prognosis, and its heterogeneity affects the response to clinical treatments. Glycolysis is highly associated with HCC therapy and prognosis. The present study aimed to identify a novel biomarker for HCC by exploring the heterogeneity of glycolysis in HCC. The intersection of both marker genes of glycolysis-related cell clusters from single-cell RNA sequencing analysis and mRNA data of liver HCC from The Cancer Genome Atlas were used to construct a prognostic model through Cox proportional hazard regression and the least absolute shrinkage and selection operator Cox regression. Data from the International Cancer Genome Consortium were used to validate the results of the analysis. Immune status analysis was then conducted. A significant gene in the prognostic model was identified as a potential biomarker and was verified through *in vitro* experiments. The results revealed that the glycolysis-related prognostic model divided patients with HCC into high- and low-risk groups. A nomogram combining the model and clinical features exhibited accurate predictive ability, with an area under the curve of 0.763 at 3 years. The high-risk group exhibited a higher expression of checkpoint genes and lower tumor immune dysfunction and exclusion scores, suggesting that this group may be more likely to benefit from immunotherapy. The tumor tissues had a higher zinc finger protein (ZFP)41 mRNA and protein expression compared with the adjacent tissues. *In vitro* analyses revealed that ZFP41 played a crucial role in cell viability, proliferation, migration, invasion and glycolysis. On the whole, the present study demonstrates that the glycolysis-related prognostic gene, ZFP41, is a potential prognostic biomarker and therapeutic target, and may play a crucial role in glycolysis and malignancy in HCC.

Correspondence to: Professor Bei Li or Professor Hui Ye, Division of Biliary Tract Surgery, Department of General Surgery, West China Hospital, Sichuan University, 37 Guoxue Alley, Wuhou, Chengdu, Sichuan 610041, P.R. China
E-mail: nanshengcheng@yeah.net
E-mail: yehuimd@163.com

Abbreviations: HCC, hepatocellular carcinoma; scRNA-Seq, single-cell RNA sequencing; LIHC, liver hepatocellular carcinoma; TCGA, The Cancer Genome Atlas; LASSO, least absolute shrinkage and selection operator; ICGC, International Cancer Genome Consortium; TIDE, tumor immune dysfunction and exclusion; OS, overall survival; GO, Gene Ontology; ROC, receiver operating characteristic; AUC, area under the curve; ssGSEA, single-sample gene set enrichment analysis; CCK-8, Cell Counting Kit-8; PCA, principal component analysis; t-SNE, t-distributed stochastic neighbor embedding

Key words: ZFP41, glycolysis, hepatocellular carcinoma, biomarker, scRNA

Introduction

Hepatocellular carcinoma (HCC) is an aggressive type of cancer with high morbidity and mortality rates (1-3). Glycolysis is highly associated with the prognosis of patients with HCC and plays a crucial role in the origin, proliferation and metastasis of HCC (4). On the one hand, the activation of glycolysis enhances the ability of cells to compete for energy as it accelerates glucose consumption. On the other hand, numerous metabolic intermediates accumulate in this process and facilitate the synthesis of biomacromolecules, such as nucleic acids (5). Glycolysis also produces lactate and hydrogen ions (H+), which lead to the acidification of immune microenvironments and inhibit immune cell function (6). Therefore, the genomics of glycolysis may be aid in the identification of novel prognostic biomarkers.

Given that HCC is a highly heterogeneous tumor (7,8), some relatively weak yet important signals on glycolytic signaling pathways in the liver may be missed by conventional sequencing techniques. Single-cell RNA sequencing analysis (scRNA-Seq) is an excellent technique used to explore the genetic information in specific cell clusters in tumor tissues of a patient (9,10). This technique has more genetic information and less background interference than traditional gene sequencing, and is helpful for exploring new prognostic factors and avoiding omission of important genetic information.

The present study explored the heterogeneity of glycolysis states in HCC tissues through scRNA-seq and constructed

a glycolysis-related prognostic model to predict prognosis and response to immunotherapy. The most significant gene, zinc finger protein (ZFP)41, in the model was identified as a potential biomarker of HCC. Further analyses and experiments were conducted to investigate the characteristics and prognostic value of ZFP41 in HCC. The present study aimed to identify a novel prognostic biomarker and therapeutic target from glycolysis-related model construction and experimental verification and provide new perspectives into the underlying molecular mechanisms of HCC.

Materials and methods

Acquisition of glycolysis-related genes. A total of 198 glycolysis-related genes were identified in the Molecular Signatures Database of the human Gene Set HALLMARK_GLYCOLYSIS. (https://www.gsea-msigdb.org/gsea/msigdb/human/geneset/HALLMARK_GLYCOLYSIS).

Ethics approval. The present study and all included experimental procedures were approved by the Biomedical Ethics Review Committee, West China Hospital, Sichuan University (Chengdu, China; Approval no. 2023-0121 and no. 2020-1866). For the experimental procedures involving tissues from human participants, exemption for patient consent was granted by the Biomedical Ethics Review Committee, West China Hospital, Sichuan University.

scRNA-seq data download and processing. GSE146115, which contains 16 samples from 4 patients, was downloaded from the Gene Expression Omnibus database for liver hepatocellular carcinoma (LIHC). Each patient provided four samples, each from one part of a tumor. Data quality control was conducted using the R package 'Seurat'. The cells selected had <5% mitochondrial genes, a total number of >50 genes and genes were expressed in at least three cells. For the following analysis, 1,500 variable genes were selected in each cell after normalizing their expression. Principal component analysis (PCA) was performed by setting the number of PCs to 20. k-Nearest neighbor (KNN) was calculated based on 20 previous PCs and the resolution was set to 0.5 for the purpose of clustering cells and further reducing the dimension by using t-distributed stochastic neighbor embedding (t-SNE). The reference dataset built into the 'SingleR' function in R was used to to automatically annotate each cell cluster. The reference data set includes BlueprintEncodeData Blueprint (11) and Encode (12), HumanPrimaryCellAtlasData the Human Primary Cell Atlas (13), DatabaseImmuneCellExpressionData The Database for Immune Cell Expression(/eQTLs/Epigenomics) (14). Glycolysis genes were imported into each cell through the 'PercentageFeatureSet' function to determine their percentage. A feature violin plot was used to illustrate the percentage of glycolytic genes in each cell or cluster.

Downloading and manipulation of transcriptome with clinical data. The transcriptome data of 374 patients with LIHC and corresponding clinical information were retrospectively collected from The Cancer Genome Atlas (TCGA) data portal (https://portal.gdc.cancer.gov/) as the training cohort. Moreover, 273 samples from the International Cancer Genome Consortium (ICGC) data portal with clinical information were downloaded as the validation cohort (https://dcc.icgc.org/projects/LIRI-JP). The TPM data type was extracted from raw data and used for subsequent analysis.

Construction of the prognostic model associated with glycolysis. Differentially expressed differentially between the 374 LIHC samples and 50 normal samples were identified using the R package 'limma' according to the criteria of a fold change >1 and false discovery rate <0.05 in TCGA cohort. Univariate Cox proportional hazard regression analysis was applied to assess the association between gene expression and the overall survival (OS) of patients with HCC. Least absolute shrinkage and selection operator (LASSO) Cox regression was used to identify the fewest genes with the most complete information. Highly correlated genes were identified among the LASSO genes, and a prognostic gene signature was constructed using multivariate Cox proportional hazard regression. The risk score of patients was calculated according to the expression of each glycolysis-related gene and its corresponding regression coefficient by using the following formula: $\text{RiskScore}=e^{\text{sum (each gene's expression x corresponding coefficient)}}$. TCGA cohort was divided into the low- and high-risk groups based on its median risk score. The R packages 'survival' and 'survivalROC' were used to determine the survival rates of the patients in the high- and low-risk groups and evaluate accuracy of the prognostic model. A two-stage test was applied when late-stage crossover appeared in survival curves using the R package 'TSHRC' to obtain the P-values for survival analysis. A P-value <0.05 was considered to indicate a statistically significant difference.

External validation of the glycolysis-related gene signature model. LIRI-JP in the ICGC data portal was selected to validate the glycolysis-related prognostic model. In the ICGC validation cohort, the risk scores of each patient were calculated using the formula of the model, and patients were divided into the high- and low-risk groups based on the median risk score of TCGA cohort. Survival analysis was performed to determine differences in prognosis between the two subgroups in the validation cohort. A receiver operating characteristic (ROC) curve was used to evaluate the accuracy of the model.

Construction of a nomogram. TCGA cohorts were used for the subsequent analysis. A nomogram was constructed to assess the risk of mortality in patients by combining clinical data and the prognostic model. The accuracy of the nomogram was evaluated in estimating the outcomes of patients using prognostic ROC curves.

Functional enrichment analysis. By using the 'clusterProfiler' R package, the Gene Ontology (GO) enrichment analyses for different risk groups was examined to identify biological functions and signaling pathways associated with them. The parameter minGSSize was set to 10 and maxGSSize was set to 500. A P-value <0.05 was considered to indicate a statistically significant difference.

Immune status analysis. The single-sample gene set enrichment analysis (ssGSEA) score was employed by using the R package 'GSVA' to quantify the activity or enrichment levels

of immune cells and immune functional pathways in HCC samples. An FDR <0.05 was regarded as statistically significant. Differences between the high- and low-risk groups were investigated in terms of immune cell infiltration to determine immune cells with different functional scores. In the two subgroups, the expression of immune checkpoint genes was analyzed using the Wilcoxon test. Immune exclusion ability and tumor immune dysfunction and exclusion scores of LIHC were calculated based on the database tumor immune dysfunction and exclusion (TIDE; http://tide.dfci.harvard.edu/login/).

Survival analysis and clinical correlation analysis. The expression of ZFP41 combined with survival data was analyzed using the R package 'survival', and Kaplan-Meier curves were drawn. The association between the expression of ZFP41 and clinical data was determined.

HCC tissue collection. A total of 22 pairs of liver cancer tissues for reverse transcription-quantitative PCR (RT-qPCR) and eight pairs of HCC specimens were obtained from patients who underwent hepatectomy and pathologically diagnosed with HCC from March, 2020 to December, 2023 at the Department of Biliary Surgery, West China Hospital of Sichuan University, Chengdu, China. The patients did not receive any pre-operative chemoradiotherapy. The clinical and pathological characteristics of the patients are presented in Table SI.

Validation of mRNA expression. Primer series of ZFP41 were designed according to gene sequence on https://blast.ncbi.nlm.nih.gov/Blast.cgi. Two pairs of primers were successfully designed: Primer2 (forward, 5'-TAAGCACAAGACAGACCACATTC-3' and reverse, 5'-GAGATTGGAGCCGCAGTTAAAG-3') and primer4 (forward, 5'-GAGTGTGGGCGGATCTTTAAG-3' and reverse, 5'-ATGTTTCAGGAGATTGGAGCC-3'). The verification results of each pair of primers were similar in the pre-experiments, which ensured the accuracy and authenticity of the subsequent verification results. TRIzol® LS reagent (Invitrogen; Thermo Fisher Scientific, Inc.) was used to extract mRNA and the reverse transcription of total cDNA from HCC tissues and adjacent tissues was conducted using a PrimeScript RT Reagent kit (Bio-Rad Laboratories, Inc.). qPCR was conducted using the qRT-PCR instrument BioRad CFX96 and the BeyoFast™ SYBR-Green One-Step qRT-PCR kit (Bio-Rad Laboratories, Inc.). Pre-denaturation in 95˚C lasted for 2 min. There are total of 39 cycles in thermal cycling protocol used for RT-qPCR; one cycle included 95˚C for 15 sec, 60˚C for 15 sec and 72˚C for 30 sec. The melt curve stage was added at the end. All RNA expression levels were standardized using the reference gene, β-actin (primer sequence: Forward, 5'-AGCGCGGCTACAGCTTCACC-3' and reverse, 5'-AGCAGCCGTGGCCATCTCTT-3') and processed using the $2^{-\Delta\Delta Cq}$ method (15).

Validation of prognostic gene protein expression. Immunohistochemical staining was conducted to verify the differences in the ZFP41 protein expression level between HCC tissues and para-carcinoma tissues. All the HCC specimens were preserved in 10% formalin at room temperature, embedded in paraffin and cut into sections at a thickness of 5 μm. EDTA (cat. no. P0085, Beyotime Institute of Biotechnology) (pH 8.0) was used to conduct antigen retrieval. The sections were blocked with 3% hydrogen peroxide for 15 min at room temperature. The primary antibody, ZFP41 polyclonal antibody (cat. no. PA5-63276), was obtained from Invitrogen; Thermo Fisher Scientific, Inc. and were diluted at a ratio of 1:500 for overnight incubation at 4˚C. Goat anti-rabbit immunoglobulin (1:200 diluted; cat. no. 31466; Invitrogen; Thermo Fisher Scientific, Inc.) was used for 40 min for secondary antibody incubation at room temperature after blocking with goat serum (Invitrogen; Thermo Fisher Scientific, Inc.) for 30 min at room temperature. DAB (Beyotime Institute of Biotechnology) color development for 45 sec and hematoxylin (Beyotime Institute of Biotechnology) counterstaining for 15 sec were then performed at room temperature. A Nikon inverted microscope (Nikon Corp.) was used to obtain images of the sections after sealing. The average optical density of each image was analyzed using ImageJ software (version 1.45s/Java1.6.0_20, National Institutes of Health) to present the protein expression of ZFP41.

Cells, cell culture and transfection. The Huh7 and PLC cell lines (cat. no. CL-0120, cat. no. CL-0415; Procell Life Science &Technology Co., Ltd.) were derived from the cell bank of Research Center for Biliary Diseases, West China Hospital of Sichuan University. Both cell lines were maintained in Dulbecco's modified Eagle's medium (DMEM, HyClone; Cytiva) supplemented with 10% fetal bovine serum (FBS, HyClone; Cytiva) and 1% streptomycin-penicillin (HyClone; Cytiva). According to the multivariate Cox proportional hazard regression analysis (the RiskScore formula below) and single-gene survival analysis (as shown below), ZFP41 was the gene with the highest coefficient and efficient survival outcomes. Blank vectors pLKO.1 were used to construct vectors with short hairpin RNAs. Blank vectors pCDH were used to construct vectors with the overexpression sequence. pLKO.1 and pCDH were obtained from Frontiers Science Center for Disease-related Molecular Network, West China Hospital of Sichuan University. Cells were transfected with the previously synthesized short hairpin RNAs (target sequence: sh2, GGGAGAGAAGCCCTTCAAA; sh4, CCCTACGAATGCACGCACTGT) and overexpression sequence (GAGTGTGGGCGGATCTTTAAG) targeting gene ZFP41 by using Lipofectamine 3000® reagent (Invitrogen; Thermo Fisher Scientific, Inc.) according to the manufacturer's protocol. The cells were transfected with blank vectors (pLKO.1 or pCDH) to serve as negative controls for the experiments. The scrambled sequence in pLKO.1 was CCTAAGGTTAAGTCGCCCTCG. The shRNA and overexpression sequences for the ZFP41 gene are provided in Table SII. Second-generation lentiviral transduction was performed. psPAX2 (1,000 ng/μl, Delivectory Biosciences Inc.) and pMD2.G (1,000 ng/μl, Delivectory Biosciences Inc.) were used as packaging vectors. 293T cells (cat. no. CL-0005; Procell Life Science & Technology Co., Ltd.) at a density of 70% were transfected with a mixture of the 3 transfection vectors (psPAX2:pMD2.G:constructed vectors=0.3125:0.3125:1.875 μg). Lipofectamine 3000® reagent (Invitrogen; Thermo Fisher Scientific, Inc.) was used at a mass ratio of 1:2 (DNA:Lipofectamine 3000). The medium was replaced with fresh medium was following overnight incubation at 37˚C with 5% CO_2. The viral supernatant was collected

after 48 h and centrifuged at 500 x g for 5 min at 4˚C to pellet the lentiviral particles. The PLC and Huh7 cells (40% confluency) were then respectively infected with different lentiviral particles at a multiplicity of infection of 1.5 and incubated with virus at 37˚C for 48 h. The medium was then replaced with fresh medium with 3 μg/ml puromycin (cat. no. A1113802, Thermo Fisher Scientific, Inc.) once every 2 days for 4 days to obtain stable cell lines. The mRNA expression of ZFP41 in the different transfected cells was verified and stable cell lines successfully constructed were used in the following experiments.

Cell Counting Kit-8 (CCK-8) assay. The CCK-8 (Biosharp Life Sciences) assay was used to detect cell viability. For each cell line, five types of transfected cells were seeded into 96-well cell culture plate with the same cell density (1,500 cells per well) and CCK-8 solution was added (10 μl per 100 μl of the FBS-free medium) for different durations (24, 48, 72 and 96 h). The cells were preserved in CO_2 incubator for 1 h and the absorbance at an optical density of 450 nm wavelength was detected using a microplate reader (BioTek Instruments, Inc.). All data are presented as the mean ± SD of five independent experiments.

Clone formation assay. Clone formation assay was used to detect the cell proliferative ability. The transfected cells were seeded into a six-well cell culture plate with the same cell density (500 cells per well). The cells were preserved in a CO_2 incubator for 14 days, and the medium was replaced every 3 days. The cells were then rinsed with PBS, fixed with methanol for 20 min and stained with 0.1% crystal violet (cat. no. C0121-500ml, Beyotime Institute of Biotechnology) for 10 min at room temperature, and photographed using a digital camera (PowerShot G7 X Mark II, Canon). The average area of cell clusters in the images was analyzed using ImageJ software (version 1.45s/Java1.6.0_20, National Institutes of Health). All data are presented as the mean ± SD of five independent experiments.

Scratch wound healing assay. Scratch wound healing assay was used to detect the horizontal migration of the cells. The transfected cells were fully seeded into a six-well cell culture plate. When the cells adhered to the wall, a scratch wound was made gently with a 1,000-μl pipette tip. The medium was replaced with serum-free medium. The cells were preserved in a CO_2 incubator for 48 h. The scratch wound was photographed using a Nikon inverted microscope (Nikon Corp.) at 0, 24 and 48 h. The healing area of the cells in the images was marked and analyzed using ImageJ software (version 1.45s/Java1.6.0_20, National Institutes of Health). All data are presented as the mean ± SD of five independent experiments.

Transwell assay. Transwell assay was used to assess the migratory capacity of the cells. In brief, 0.2 ml of the transfected cells resuspended in serum-free medium ($2.5x10^4$ cells per ml) were seeded into a Transwell chamber (Corning, Inc.) on a 24-well culture plate with 0.6 ml DMEM combined with 20% FBS. After the cells were preserved in a CO_2 incubator for 48 h, they were rinsed with PBS, fixed with methanol for 20 min and stained with crystal violet for 10 min at room temperature. The cells were photographed using a Nikon inverted microscope (Nikon Corp.) and analyzed using ImageJ software (version 1.45s/Java1.6.0_20, National Institutes of Health). All data are presented as the mean ± SD of five independent experiments.

Glycolysis-related analysis. In TCGA cohort, the mRNA expression of 10 known key genes of anaerobic glycolysis (ALDOA, ENO1, GAPDH, HK2, LDHA, PFKL, TIGAR, PGK1, PKM and SLC2A1) were extracted to conduct co-expression analysis with ZFP41 using simple linear regression analysis Glucose uptake experiments and lactic acid production experiments were performed. The Glucose Uptake Cell-based Assay kit (cat. no. 600470, Cayman Chemical Co.) and Lactic Acid (LA) Content Assay kit (cat. no. BC2235, Beijing Solarbio Science & Technology Co., Ltd.) were used to examine the glycolysis status of the transfected cells. For each cell line, five types of transfected cells were seeded into 96-well cell culture plate with the same cell density ($1x10^5$ cells per well). When the cells adhered to the wall, 200 μl glucose-free medium with 100 μg/ml 2-NBDG (Cayman Chemical Co.) were added. The cells were preserved in a CO_2 incubator for 16 h. Fluorescein (excitation/emission=485/535) was detected after rinsing with Cell-based Assay Buffer (Cayman Chemical Co.). For each cell line, five typs of $5x10^6$ transfected cells were processed according to the protocol provided with the Lactic Acid (LA) Content Assay kit protocol. The absorbance at an optical density of 570 nm wavelength was detected using a microplate reader (BioTek Instruments, Inc.). All data are presented as the mean ± SD of five independent experiments.

Statistical analysis. GraphPad Prism software (version 9.0; GraphPad Software, Inc.), SPSS software (version 25.0; IBM Corp.) and R (version 4.0.5, R Foundation for Statistical Computing, Vienna, Austria) were utilized to conduct statistical analyses and plot the diagrams. A two-stage test was applied when the survival curves crossed over using the R package 'TSHRC'. The Wilcoxon rank sum test was used to reveal the differences in ZFP41 expression between adjacent normal tissue and tumor tissue. Each experiment was repeated independently at least three times. An unpaired Student's t-test and one-way ANOVA were used to assess the differences between groups. Tukey's test was used as A post hoc test for multiple comparisons. A P-value <0.05 was considered to indicate a statistically significant difference.

Results

scRNA-Seq data analysis. Following quality control and normalization, PCA was conducted on the scRNA-Seq data of LIHC GSE146115. As shown in Fig. 1A, four samples were distinguished on the dimensions of PC1 and PC2. The whole data were divided into 20 PCs with a P-value <0.001 (Fig. 1B). All cells were clustered into 11 clusters using the k-Nearest Neighbor (KNN) clustering algorithm and were presented as t-SNE diagrams. The cell type annotation of each cluster was determined using the R package 'SingleR' (Fig. 1C). Subsequently, 198 genes related to glycolysis were input using the 'PercentageFeatureSet' function to determine the percentage of glycolysis genes in each cell. The cells were divided into low- and high-glycolysis cells according to their

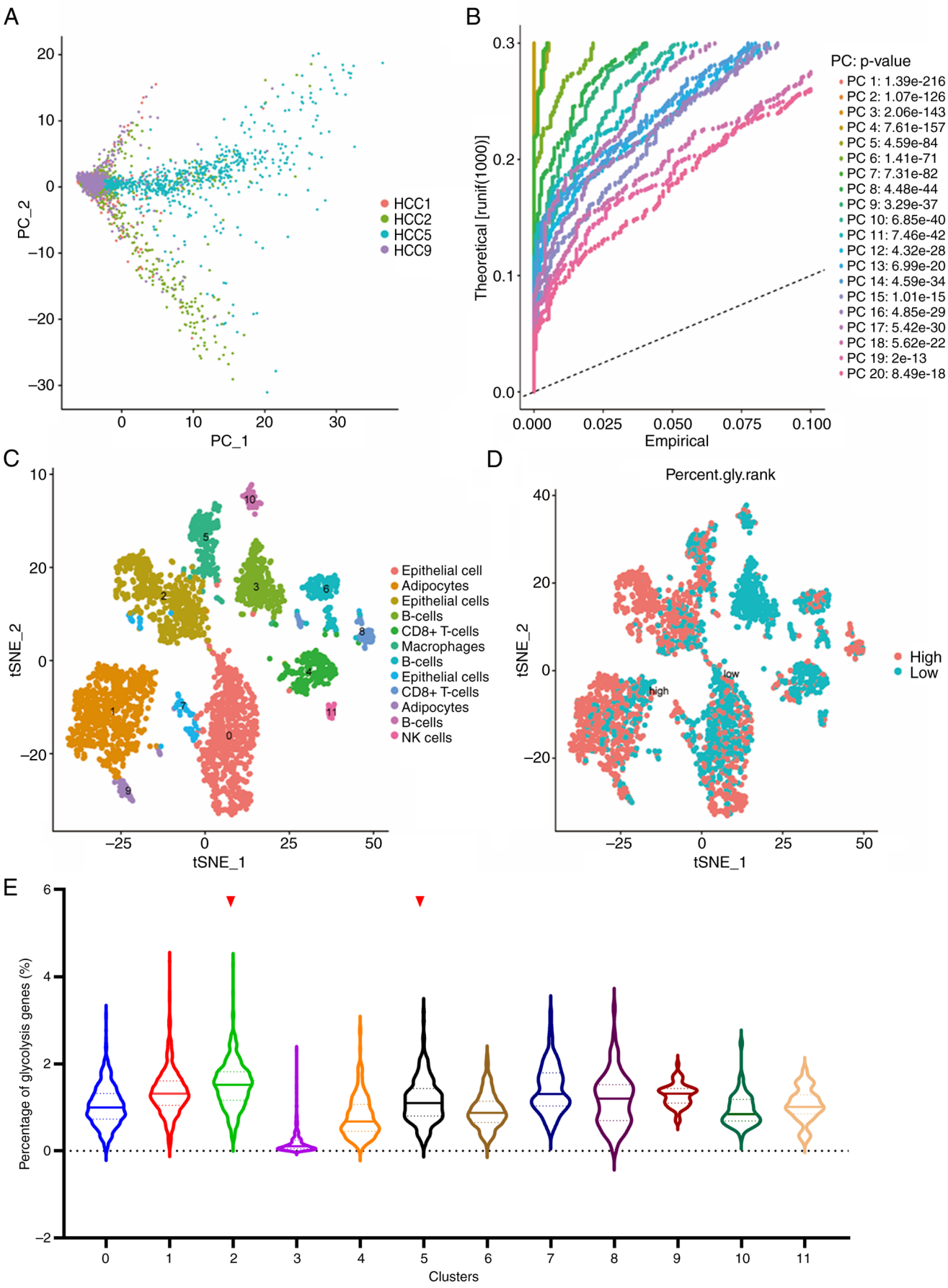

Figure 1. Single-cell sequencing analysis of GSE146115. (A) Four samples can be basically distinguished on the dimensions of PC1 and PC2. (B) The whole data can be divided into 20 principal components with a P-value <0.001. (C) All cells were clustered into 11 clusters by the k-Nearest Neighbor (KNN) clustering algorithm. (D) Cells were divided into low and high glycolytic cells by their median glycolysis gene proportion and are displayed by t-distributed stochastic neighbor embedding diagrams. (E) Percentage of glycolysis genes in each cluster was showed by the violin diagram.

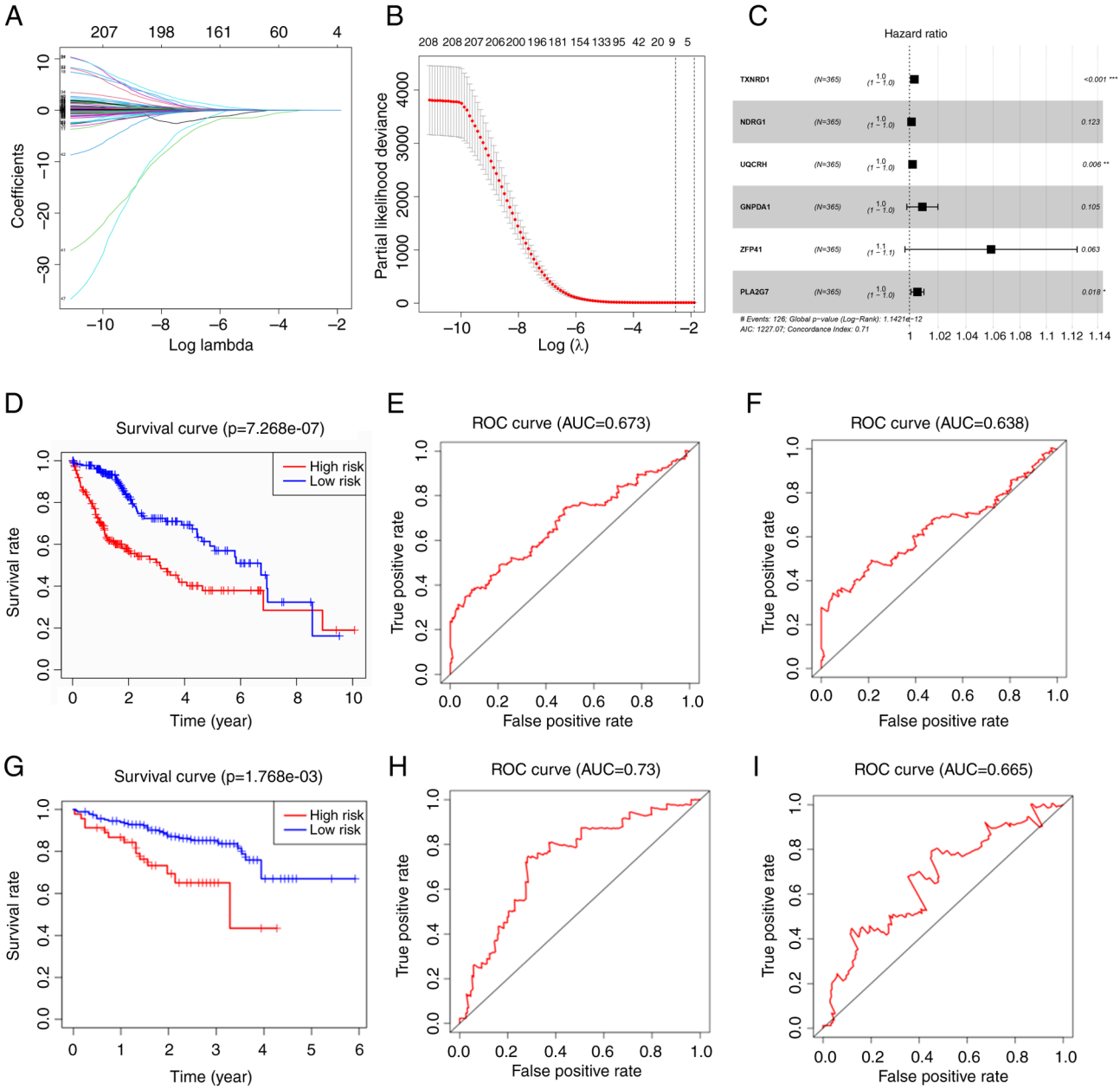

Figure 2. Construction and validation of glycolysis-related prognostic model. (A and B) Results of LASSO Cox regression analysis of 208 genes associated with survival. (C) Multivariate Cox regression analysis result of the LASSO genes. (D) Survival curves of high-risk group vs. a low-risk group based on TCGA data, according to the median risk score. (E) ROC curves and AUC value at 3 years based on TCGA data according to 6 genes model (F) ROC curves and AUC value at 5 years based on TCGA data according to 6 genes model. (G) Survival curves of the high-risk group vs. the low-risk group based on ICGC data, according to the median risk score. (H) ROC curves and AUC value at 3 years based on ICGC data according to 6 genes model (I) ROC curves and AUC value at 5 years based on ICGC data according to 6 genes model. LASSO, least absolute shrinkage and selection operator; TCGA, The Cancer Genome Atlas; ROC, receiver operating characteristic; ICGC, International Cancer Genome Consortium; AUC, area under the curve.

median glycolysis gene proportion and were displayed in the t-SNE diagram and the violin diagram (Fig. 1D and E). Comprehensively, Cluster1, Cluster2, Cluster5, Cluster8 and Cluster9 expressed more glycolysis genes. These cells were adipocytes, epithelial cells, macrophages and $CD8^+$ T-cells, respectively. Finally, the marker genes of cluster2 and cluster5 were selected, considering that cells in the liver mainly consist of hepatocytes and Kupffer cells, whose function is similar to that of epithelial cells and macrophages.

Construction and validation of glycolysis-related prognostic model. A total of 1,167 marker genes were selected and only 384 genes had a differential expression between the normal and tumor groups. A total of 208 genes were associated with OS on univariate Cox regression analysis. LASSO Cox regression analysis was then conducted with the remnant candidates that were found to be highly associated with survival, resulting in eight genes remaining (LASSO genes) (Fig. 2A and B). The LASSO genes included TXNRD1, NDRG1, UQCRH, GNPDA1, ZFP41, PSMD1, SSB and PLA2G7. These were applied in multivariate Cox regression analysis, and a prognostic model with six genes was constructed (Fig. 2C). Since Fig. 2C presents the forest map with the result of multivariate Cox regression, only the six genes that comprised the risk

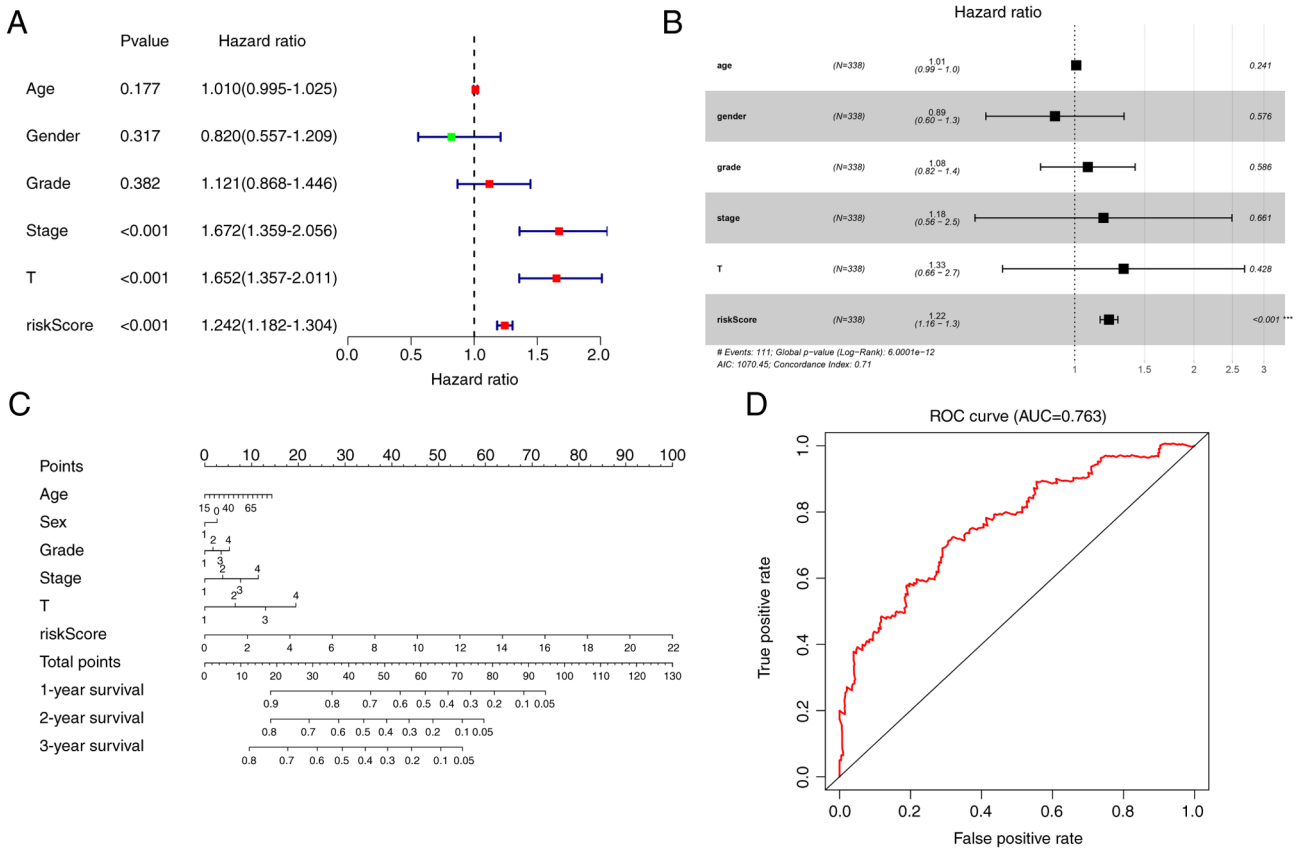

Figure 3. Construction of nomogram by analyzing TCGA cohort. (A) Results of univariate Cox analysis of clinical information and risk scores in TCGA cohort. (B) Results of multivariate Cox analysis of clinical information and risk scores in TCGA cohort. (C) A nomogram was constructed, which combined the risk score and clinical data including age, sex, grade, stage and magnitude of tumor. (D) ROC curves and AUC value at 3 years according to the nomogram. TCGA, The Cancer Genome Atlas; AUC, area under the curve.

formula in the end were displayed. The formula of the model containing six genes was as follows: RiskScore=e$^{(TXNRD1 \times 0.003395 + NDRG1 \times 0.001377 + UQCRH \times 0.002102 + GNPDA1 \times 0.008965 + ZFP41 \times 0.056787 + PLA2G7 \times 0.00548)}$. The risk score of each patient was calculated in TCGA cohort, and the patients were divided into a high- and low-risk group according to the median risk score. The Kaplan-Meier survival curve revealed that the high-risk group had poorer outcomes than the low-risk group (Fig. 2D). The model demonstrated an excellent predictive value, with areas under the curve (AUC) >0.673 at 3 years and 0.638 at 5 years (Fig. 2E and F).

The ICGC cohort was used to validate the established six-gene risk score model. The Kaplan-Meier survival curve of the high-risk group was inferior to that of the low-risk group, similar to the training cohort (Fig. 2G). The time-dependent ROC curves of the validation cohort revealed higher prediction value with AUC values >0.73 at 3 years and 0.665 at 5 years (Fig. 2H and I).

Independent prognostic value of the six-gene signature. Univariate and multivariate Cox analyses were conducted to determine whether the risk score can be an independent prognostic factor. Univariate Cox analysis revealed that the risk score was significantly associated with OS in TCGA cohort (hazard ratio, 1.242; 95% confidence interval, 1.182-1.304; P<0.001; Fig. 3A). Multivariate Cox analysis demonstrated that the risk score was also an independent prognostic factor, when combined with clinical information (hazard ratio, 1.22; 95% confidence interval. 1.16-1.3; P<0.001; Fig. 3B).

Construction of the nomogram. A nomogram was constructed, by combining the risk score and clinical data including age, sex, grade, stage and magnitude of tumor, to assess the survival of patients in TCGA cohort (Fig. 3C). Prognostic ROC analysis was performed to evaluate the accuracy of this nomogram. The AUC at 3 years was 0.763 (Fig. 3D).

Immune status analysis. To consider the differences between the two subgroups and provide a reference for immunotherapy, an immune status analysis was conducted to explore the immune infiltration levels (Fig. 4A). As shown in Fig. 4A, the high-risk group had higher immune infiltration levels in aDCs, APC_co_stimulation, Check-point, HLA, iDCs, Macrophages, MHC_class I, and Treg and lower levels in B_cells, Cytolytic_activity, Mast_cells, NK_cells, and Type II_IFN_Response. Furthermore, the expression levels of immune checkpoint genes (PDCD1, PDCD1LG2, CTLA4, CD80, CD86, HAVCR2, LGALS9, CD274 and VTCN1) were significantly increased in the high-risk group (Fig. 4B). The immune prediction model identified that the TIDE score was decreased in the high-risk group compared with that in the low-risk group, indicating a worse immune response and poorer outcomes following immunotherapy (Fig. 4C).

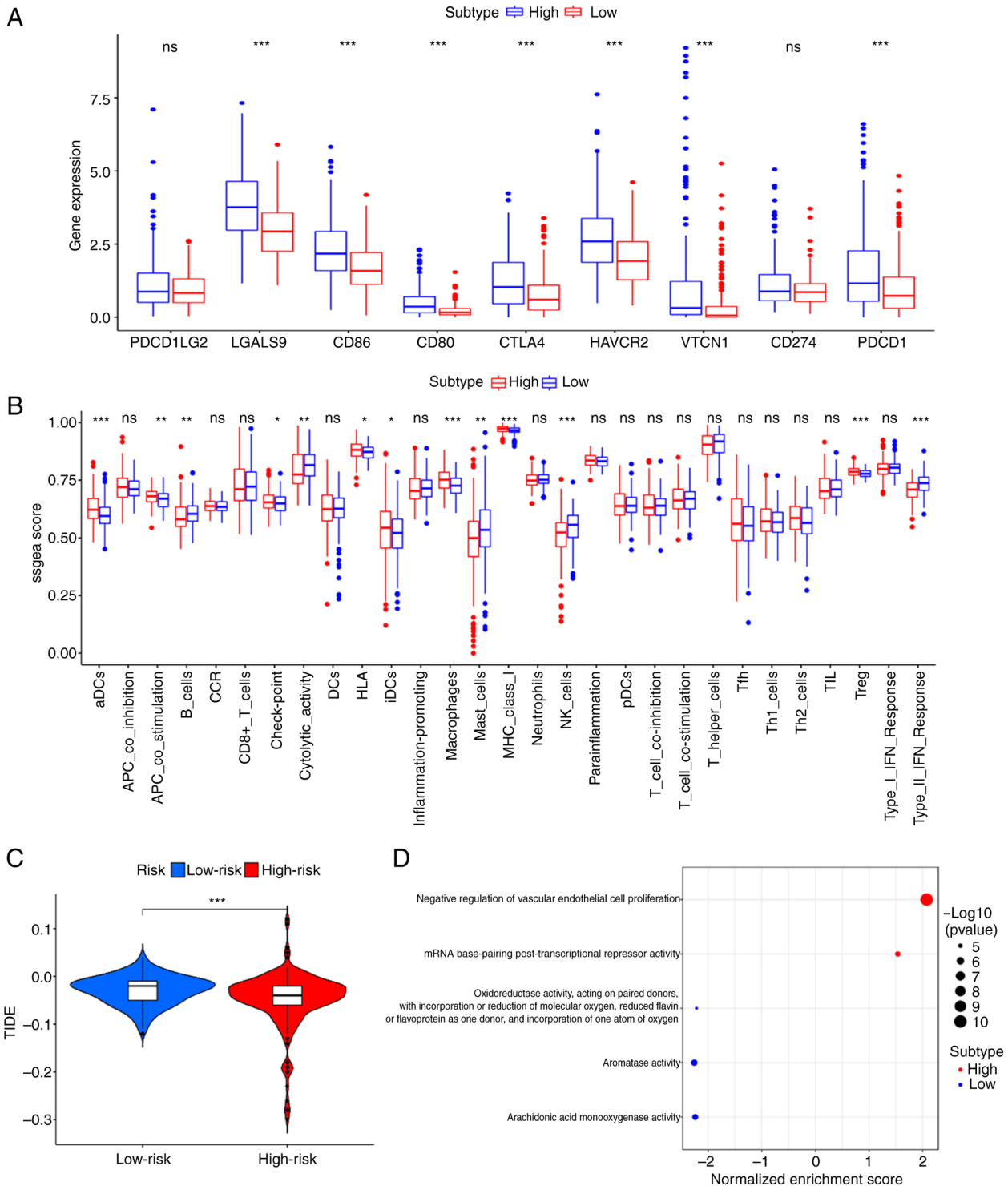

Figure 4. Immune status and function enrichment analysis of TCGA cohort based on the prognostic model. (A) The immune infiltration levels among two subgroups. Immune functions levels in aDCs, APC_co_stimulation, Check-point, HLA, iDCs, Macrophages, MHC_class I, Treg increased in high-risk group. (B) Expression level of immune checkpoint genes were significantly elevated in the high-risk group. (C) Results of capability of TIDE score of high-risk group vs. a low-risk group. (D) Results of Gene Ontology enrichment analysis according to the six-gene prognostic model. *P<0.05, **P<0.01 and ***P<0.001.

GO enrichment analysis. GO enrichment analysis was conducted using TCGA cohort to reveal the molecular mechanism of the six-gene prognostic model. As shown in Fig. 4D, two signaling pathways, including the negative regulation of vascular endothelial cell proliferation and mRNA base-pairing post-transcriptional repressor activity were markedly enriched in the high-risk group compared with the low-risk group.

Survival analysis of ZFP41. In multivariate Cox regression analysis, the coefficient of ZFP41 was the highest among the six model genes. Survival analysis was conducted on ZFP41. Patients with a high expression of ZFP41 had a significantly worse prognosis than patients with a low expression of ZFP41 (P<0.001; Fig. 5A). The expression of ZFP41 was found to be highly associated with the patient clinical characteristics,

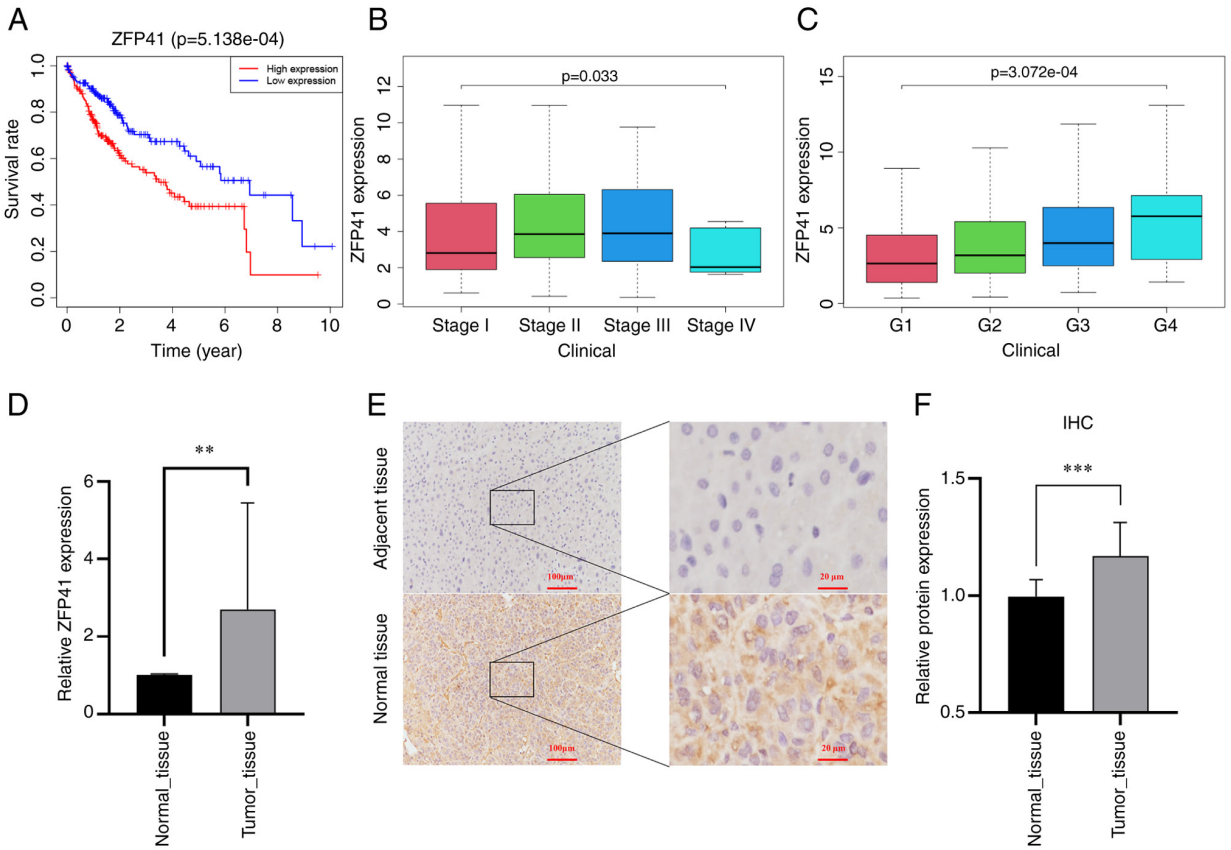

Figure 5. Exploring the prognostic and clinical value of ZFP41 in TCGA cohort and validation of its mRNA and protein expression. (A) Survival analysis results of TCGA data according to ZFP41. (B and C) Association analysis between clinical outcomes (grade and stage) and ZFP41 expression. (D) Results of reverse transcription-quantitative PCR of 22 pairs of HCC tissues. (E) Immunohistochemical staining illustrating ZFP41 protein expression between HCC and adjacent normal tissue at x10 magnification and at x50 magnification. (F) Relative ZFP41 protein expression of eight pairs of HCC specimens calculated according to optical density per area of tumor tissue and normal tissue; the data presented in (F) are based on the data presented in (E). **P<0.01 and ***P<0.001. TCGA, The Cancer Genome Atlas; HCC, hepatocellular carcinoma.

including grade (P<0.001; Fig. 5B) and the stage of LIHC (P<0.05; Fig. 5C).

High expression of ZFP41 in tumor tissues. The differences in expression levels between tumor and normal tissues were verified. A total of 22 pairs of HCC tissues were collected for RT-qPCR to detect ZFP41 gene expression, and eight pairs of HCC tissues were collected for immunohistochemical analysis to detect ZFP41 protein expression. The results of RT-qPCR revealed that the mRNA level of ZFP41 was higher in the tumor tissues (P=0.004, Fig. 5D). Immunohistochemistry revealed that the tumor tissue had a higher optical density per area than the normal tissue (P<0.001; Fig. 5F), indicating that ZFP41 protein had a higher expression in HCC tissues. Brown granules, which represented ZFP41 protein, were more commonly observed in the HCC cytoplasm and intercellular substance (Fig. 5E). The data presented in Fig. 5F (optical density) are based on the data presented in Fig. 5E (staining images).

ZFP41 plays a crucial role in Huh7 and PLC cell viability in vitro. RT-qPCR was conducted to evaluate the mRNA level of ZFP41 in Huh7 cells and assess the effects of shRNA targeting ZFP41 and overexpression plasmid for ZFP41. The mRNA expression of ZFP41 increased in the cells overexpressing ZFP41 (Huh7 cells: NC vs. OE-ZFP41, P=0.007; PLC cells: NC vs. OE-ZFP41, P<0.001; Fig. 6A and C) and decreased in the cells transfected with shRNA (SH2-ZFP41 and SH4-ZFP41; Huh7 cells: SH-NC vs. SH2-ZFP41, P=0.016; SH-NC vs. SH2-ZFP41, P=0.004; PLC cells: SH-NC vs. SH2-ZFP41, P<0.001; SH-NC vs. SH4-ZFP41, P<0.001; Fig. 6B and D).

The results of CCK-8 assay revealed that after ZFP41 was overexpressed, the viability of the Huh7 and PLC cells significantly increased (Huh7 cells: NC vs. OE-ZFP41, P<0.001; PLC cells: NC vs. OE-ZFP41, P<0.001; Fig. 6E and G). Following the knockdown of ZFP41, the Huh7 and PLC cells exhibited a reduced viability (Huh7 cells: SH-NC vs. SH2-ZFP41, P=0.006; SH-NC vs. SH2-ZFP41, P<0.001; PLC cells: SH-NC vs. SH2-ZFP41, P=0.024; SH-NC vs. SH4-ZFP41, P=0.01; Fig. 6F and H). Hence, ZFP41 plays an important role in HCC cell survival.

ZFP41 plays a crucial role in Huh7 And PLC cell proliferation in vitro. Colony formation assay was conducted to assess the proliferation of the Huh7 and PLC cells following the overexpression and knockdown of the ZFP41 gene. The average size of cell colony clusters in the ZFP41-overexpressing cells was significantly higher than that in normal cells (Huh7 cells: NC vs. OE-ZFP41, P<0.001; PLC cells: NC vs. OE-ZFP41, P=0.008; Fig. 6I and J). The average size of cell colony clusters in the shRNA-transfected cells (SH2-ZFP41 and SH4-ZFP41)

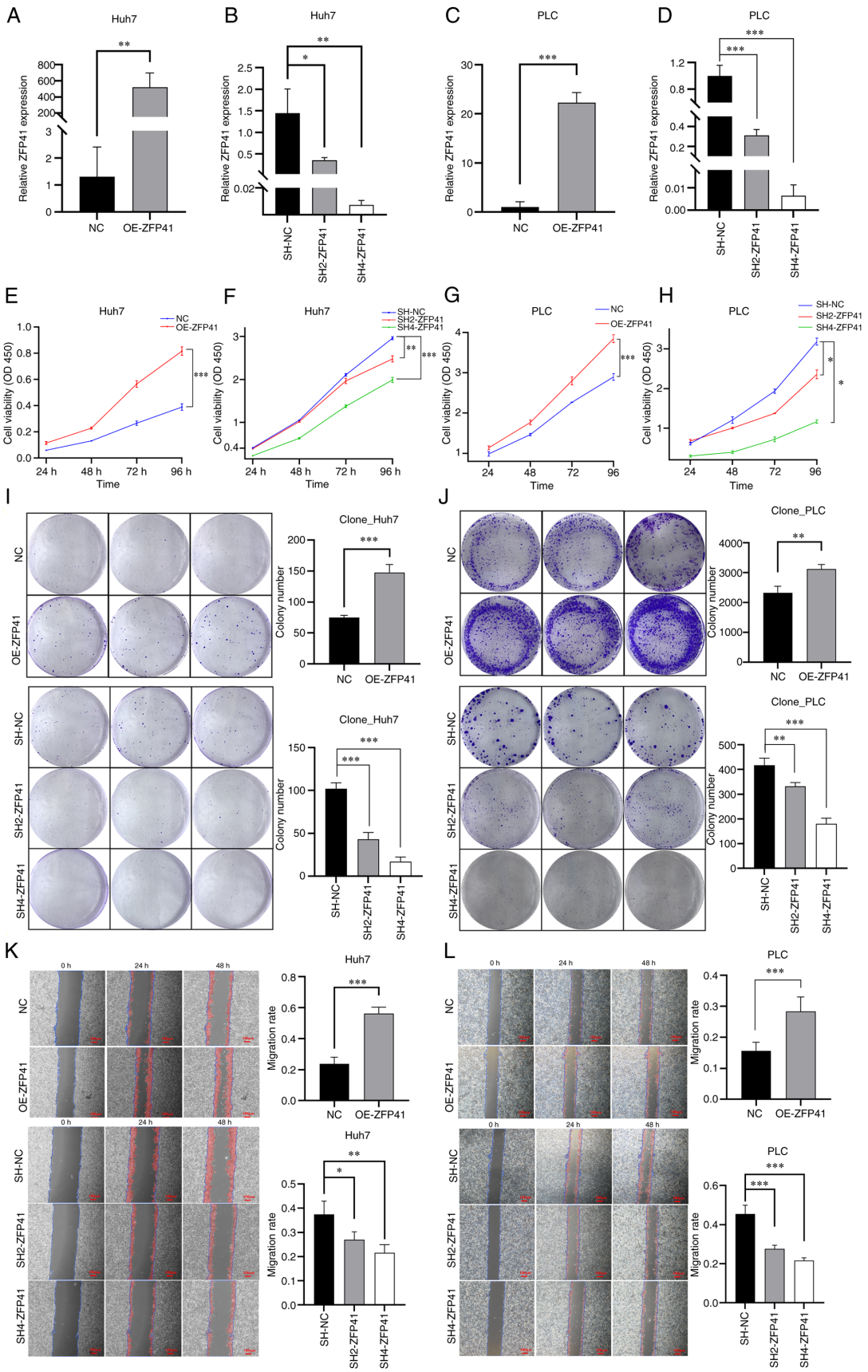

Figure 6. Effects of ZFP41 on cell viability and proliferation *in vitro*. (A and C) RT-qPCR results of OE-ZFP41 cells and normal cells (NC) in Huh7 and PLC cell lines. NC cells were cells transfected with blank vectors. (B and D) RT-qPCR results of SH2-ZFP41 cells, SH4-ZFP41 cells and NC cells (Huh7 and PLC cell lines). NC cells were cells transfected with blank vectors. (E and G) Results of CCK-8 assay of OE-ZFP41 cells and normal Huh7 cells (F and H) Results of CCK-8 assay of SH2-ZFP41 cells, SH4-ZFP41 cells and NC cells (Huh7 and PLC cell lines). (I and J) Results of colony formation assay of OE-ZFP41 cells and normal cells, and SH2-ZFP41 cells, SH4-ZFP41 cells and NC cells (Huh7 and PLC cell lines). (K and L) Results of scratch wound healing assay of OE-ZFP41 cells and NC cells, and SH2-ZFP41 cells, SH4-ZFP41 cells and NC cells (Huh7 and PLC cell lines). *P<0.05, **P<0.01 and ***P<0.001. RT-qPCR, reverse transcription-quantitative PCR; OE, overexpression; SH, shRNA.

was lower than that in normal cells (Huh7 cells: SH-NC vs. SH2-ZFP41, P<0.001; SH-NC vs. SH2-ZFP41, P<0.001; PLC, SH-NC vs. SH2-ZFP41, P=0.001; SH-NC vs. SH4-ZFP41, P<0.001; Fig. 6I and J). Hence, the results demonstrated that ZFP41 plays a crucial role in HCC cell proliferation and the SH4-RNA sequence exhibited a high knockdown efficiency.

ZFP41 plays a crucial role in Huh7 And PLC cell migration and invasion in vitro. Scratch wound healing and Transwell assays were conducted to evaluate the migratory and invasive ability of the cells following the overexpression and knockdown of the ZFP41 gene. The results of scratch wound healing assay demonstrated that the healing speed of the OE-ZFP41 cell cluster was higher than that of the normal cell cluster (Huh7 cells: NC vs. OE-ZFP41, P<0.001; PLC cells: NC vs. OE-ZFP41, P<0.001; Fig. 6K and L). The healing speed of the SH2-ZFP41 cell and SH4-ZFP41 cell clusters (cells transfected with shRNA) was lower than that of the normal cell cluster (Huh7 cells: SH-NC vs. SH2-ZFP41, P=0.016; SH-NC vs. SH2-ZFP41, P=0.001; PLC cells: SH-NC vs. SH2-ZFP41, P<0.001; SH-NC vs. SH4-ZFP41, P<0.001; Fig. 6I and J).

The density of the transfected Huh7 and PLC cells outside the Transwell chamber is illustrated in Fig. 7A and B. The density of the ZFP41-overexpressing cells outside the Transwell chamber was higher than that of the normal cell cluster (Huh7 cells: NC vs. OE-ZFP41, P<0.001; PLC cells: NC vs. OE-ZFP41, P<0.001; Fig. 7C and E). The density of the SH2-ZFP41 and SH2-ZFP41 cells (cells transfected with shRNA) outside the Transwell chamber was lower than that of the normal cell cluster (Huh7 cells: SH-NC vs. SH2-ZFP41, P<0.001; SH-NC vs. SH2-ZFP41, P<0.001; PLC cells: SH-NC vs. SH2-ZFP41, P<0.001; SH-NC vs. SH4-ZFP41, P<0.001; Fig. 7D and F). These experimental results illustrated that ZFP41 plays a crucial role in HCC cell metastasis.

ZFP41 plays a crucial role in the HCC cell glycolytic status. Co-expression analysis demonstrated the simple linear regression association between ZFP41 and certain known key genes of anaerobic glycolysis (ALDOA, ENO1, GADPH and PFKL, P<0.001; PKM, P=0.011; PGK1, P=0.021; Fig. 8A-C, F, H and I). The results of glucose uptake assay revealed that the ZFP41-overexpressing cells had a higher glucose uptake (Huh7 cells: NC vs. OE-ZFP41, P=0.007; PLC cells: NC vs. OE-ZFP41, P=0.007; Fig. 8K), and that the SH2-ZFP41 and SH2-ZFP41 cells had a lower glucose uptake (Huh7 cells: SH-NC vs. SH2-ZFP41, P=0.006; SH-NC vs. SH2-ZFP41, P<0.001; PLC cells: SH-NC vs. SH2-ZFP41, P<0.006; SH-NC vs. SH4-ZFP41, P<0.001; Fig. 8L). The results of lactic acid generation assay demonstrated that ZFP41-overexpressing cells had higher lactate generation levels (Huh7 cells: NC vs. OE-ZFP41, P=0.002; PLC cells: NC vs. OE-ZFP41, P=0.002; Fig. 8M), and the SH2-ZFP41 and SH2-ZFP41 cells had lower lactate generation levels (Huh7 cells: SH-NC vs. SH2-ZFP41, P=0.009; SH-NC vs. SH2-ZFP41, P<0.001; PLC cells: SH-NC vs. SH2-ZFP41, P=0.008; SH-NC vs. SH4-ZFP41, P<0.001; Fig. 8N). On the whole, the co-expression analysis and *in vitro* experiments indicated that ZFP41 plays a crucial role in the HCC cell glycolytic status.

Discussion

HCC is the most common primary liver malignancy and the third leading cause of cancer-related mortality worldwide (1,2,16-18). Although the targeted immunotherapy of HCC has made significant progress, the prognosis of patients with HCC remains unsatisfactory (19). One of the key reasons for the poor prognosis of patients with HCC is its high intratumor genomic heterogeneity (7,8,20). The distinctive genomic alterations, biological behavior and local microenvironments lead to different responses to similar types of immunotherapy (20). The molecular basis governing immune responses and evasion remains unclear, and validated biomarkers are not yet available to guide clinical decision making (21-23). Glycolysis plays a critical role in tumor proliferation and metastasis. Glycolysis-related genes improve the energy consumption and biomacromolecule accumulation of tumor cells, thereby affecting the tumor microenvironment and inhibiting immunity through lactate accumulation (24-26). Thus, the activated glycolysis pathway thus is highly associated with a poor prognosis and is key to the exploration of potential biomarkers.

In the present study, the scRNA data were obtained from GSE146115. The authors reconstructed single-cell and single-variant clonal evolution in human HCC in the original study of this dataset (27). It served as a reference for the investigation of the heterogeneity of glycolysis in HCC. In the present study, HCC cells were categorized based on their distinct glycolytic states. Previous research has demonstrated that monocytes display great heterogeneity among various tumors and control tumor malignancy and that stromal cells can modulate tumor stiffness and facilitate cancer progression by secreting relevant factors to the extracellular matrix (10). The activation of glycolysis in macrophages and endothelial cells can regulate the development of HCC, which is associated with a poor prognosis (28-30). Consistent with previous findings, the present study found that macrophages and endothelial cells presented higher glycolytic state. Their marker genes were selected to construct a prognostic model. The glycolysis model combined with clinical features can accurately assess the prognosis of patients with HCC with an AUC >0.763.

To explore the regulatory mechanisms of the glycolysis model, immune state analysis was conducted. The high-risk group had higher levels of aDCs, APC_co_stimulation, check-point, HLA, iDCs, Macrophages, MHC class I and Tregs. These cells have been reported to promote immune tolerance and immunosuppression, which are associated with a poor prognosis (30-36). Moreover, B cells, Cytolytic activity, Mast cells, NK cells and Type II IFN Response were lower in the high-risk group. Their levels reflected the antitumor effect by inhibiting cell proliferation, and inhibiting angiogenesis and promoting apoptosis (37-39). These findings suggest that the risk score reflects the immunosuppressive microenvironment of HCC. To determine the effect of immunotherapy, the expression of checkpoint genes was examined. In tumor cells, checkpoint genes can suppress antitumor immune responses in solid tumors (35), and immune-checkpoint inhibitors can provide clinical benefits (40). Fu *et al* (41) established a large-scale model to predict the response to immunotherapy, where a lower TIDE score predicted a higher possibility to respond to immunotherapy. In the present study, it was found that high-risk group had higher expression levels of checkpoint genes. The immune predicting model indicated that the high-risk group had lower TIDE scores. These results demonstrated that the high-risk group may be more likely to benefit from immunotherapy.

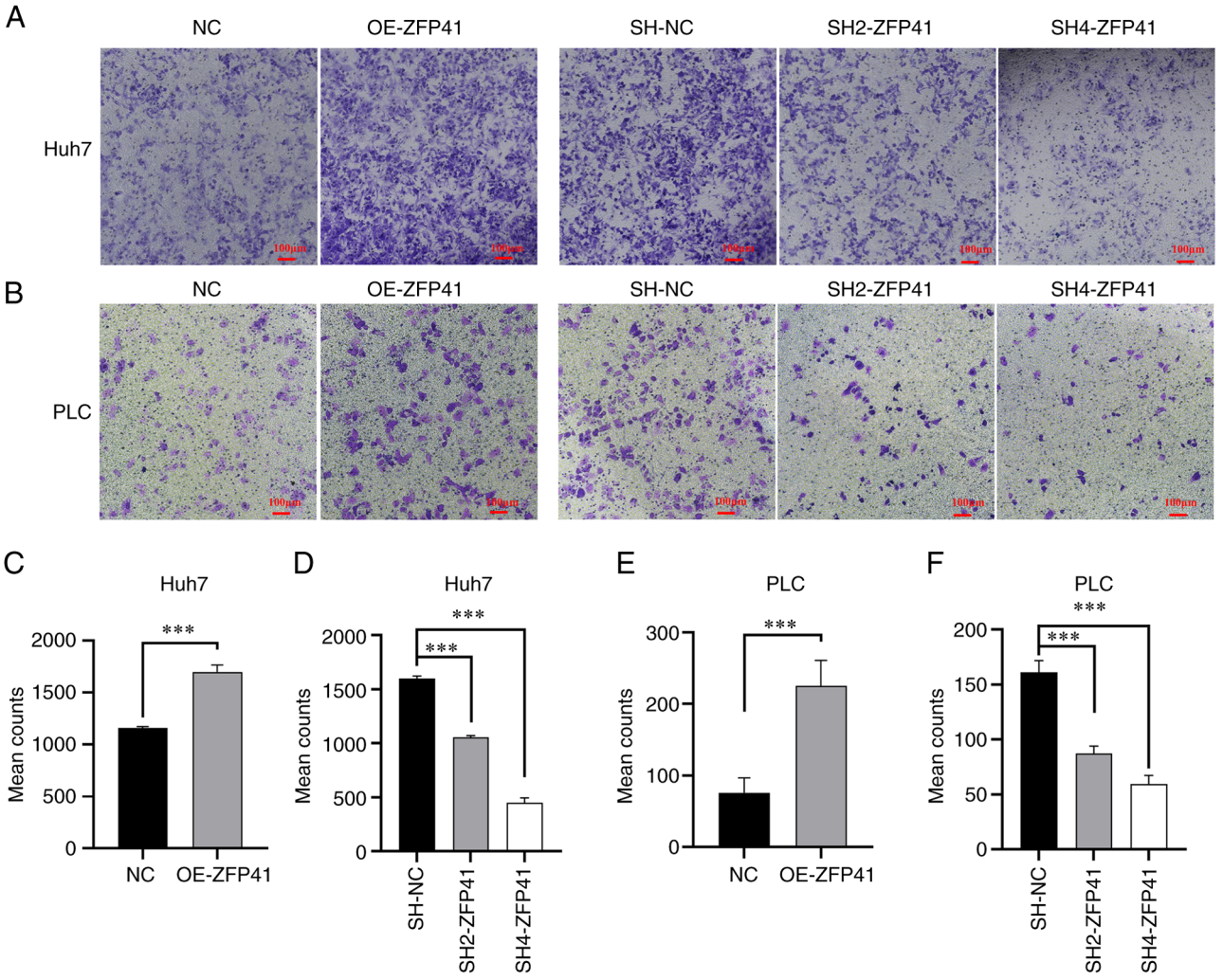

Figure 7. Effects of ZFP41 on cell migration and invasion *in vitro*. (A, C and D) Results of Transwell assay of OE-ZFP41 cell and normal cells, and SH2-ZFP41 cells, SH4-ZFP41 cells and NC cells (Huh7 cell line). (B, E and F) Results of Transwell assay of OE-ZFP41 cells and normal cells, and SH2-ZFP41 cells, SH4-ZFP41 cells and NC cells (PLC cell line). ***P<0.001. OE, overexpression; SH, shRNA.

Glycolysis-related gene targeting, in combination with immune checkpoint blockade, can breach the immunosuppressive microenvironment and improve immune checkpoint inhibitor therapy (42-44). In the present study, ZFP41 was found to be the key gene with the highest coefficient in the glycolysis-related model, and was associated with a poor prognosis of patients with HCC. ZFP41 is a type of ZFP, which play diverse roles in cell biological functions, such as cell differentiation, apoptosis, transcriptional regulation, cell metabolism and the immune response (45). Current studies have found that ZFP41 plays a prominent role in tumor differentiation and oxidative stress, and is closely related to the co-expression of LACM and venous thromboembolism (46-49). However, the role of ZFP41 in prognosis and cell function in HCC has not yet been discovered. To the best of our knowledge, the present study is the first to report that the high expression of ZFP41 is associated with a poor prognosis of patients with HCC. The high mRNA and protein expression of ZFP41 was verified in HCC tissues. Cell experiments confirmed that ZFP41 plays a crucial role in in cell viability, proliferation, migration and invasion. ZFP41 was also associated with ALDOA, GADPH, PFKL, PKM and PGK1, which can promote glycolysis and malignancy (50-56). The present study also explored the association between ZFP41 and glycolysis in HCC, and found that ZFP41 was a crucial factor in HCC glycolysis. These findings provide novel perspectives for the exploration of potential prognostic biomarkers and therapeutic targets for HCC.

To the best of our knowledge, the present study is the first to develop a glycolysis prognostic model of HCC using single-cell cluster analysis. The model not only provides a novel perspective on glycolysis in HCC, but may also help in the management of patients with HCC. The present study has certain limitations, however, which should be mentioned. The small sample size used in the immunohistochemical analysis may lead to a certain degree of risk of bias to the validation of ZFP41 protein expression in HCC tissues. The precise mechanisms underlying the effects of the glycolysis-related gene signature on the tumor microenvironment could not be clarified, and thus the effects of immunotherapy could not be predicted precisely. The mechanism through which the gene, ZFP41, affects HCC development remain unclear. Thus, further investigations are warranted to fully elucidate its role in HCC.

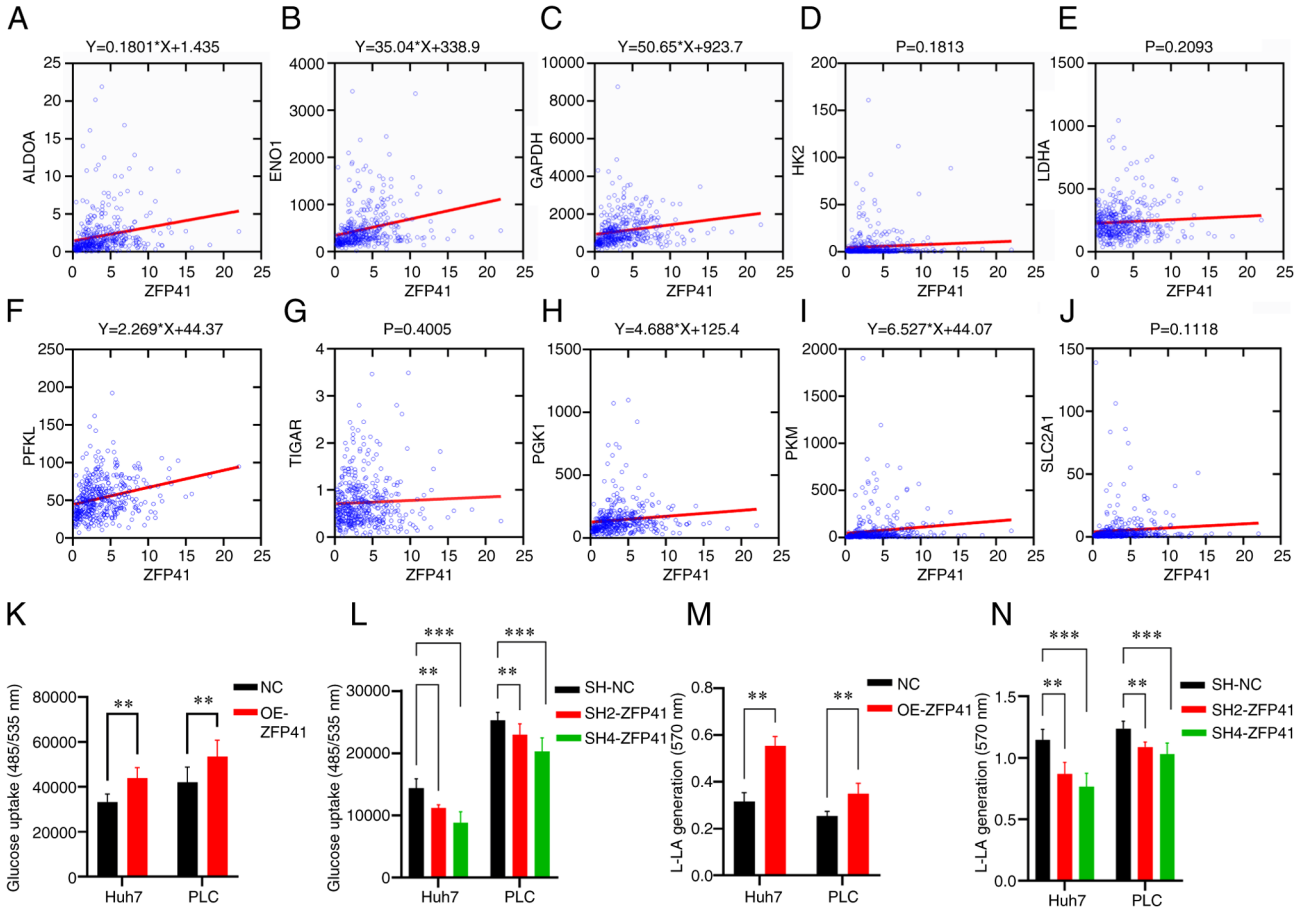

Figure 8. Association between ZFP41 and glycolysis. (A-J) Co-expression analysis between ZFP41 and 10 key glycolysis gene (ALDOA, ENO1, GAPDH, HK2, LDHA, PFKL, TIGAR, PGK1, PKM and SLC2A1). When P<0.05, a linear regression equation was drawn as the title of the diagram. (K and L) Glucose uptake cell-based assay results of OE-ZFP41 cells and NC cells, and SH2-ZFP41 cells, SH4-ZFP41 cells and NC cells (Huh7 and PLC cell lines). (M and N) Lactate generation assay results of OE-ZFP41 cells and NC cells, and SH2-ZFP41 cells, SH4-ZFP41 cells and NC cells (Huh7 and PLC cell lines). **P<0.01 and ***P<0.001. OE, overexpression; SH, shRNA.

Acknowledgements

Not applicable.

Funding

The present study was supported by the Sichuan Science and Technology Program (grant no. 2022NSFSC0680).

Availability of data and materials

The datasets generated during and/or analyzed during the bioinformatic parts of the present study are available from the public databases: GEO (https://www.ncbi.nlm.nih.gov/geo/), TCGA (https://portal.gdc.cancer.gov/) and ICGC (https://dcc.icgc.org/). The other datasets used and/or analyzed during the current study are available from the corresponding author on reasonable request.

Authors' contributions

YT, JX, YW, NW, BL and HY contributed to the conception and design of the study. Material preparation, data collection and analysis were performed by YT, JX, YW, NW, BL and HY. The first draft of the manuscript was written by YT and all authors commented on previous versions of the manuscript. YT and JX confirm the authenticity of all the raw data. All authors have read and approved the final manuscript.

Ethics approval and consent to participate

The present study and all included experimental procedures were approved by the Biomedical Ethics Review Committee, West China Hospital, Sichuan University (Chengdu, China; Approval no. 2023-0121 and no. 2020-1866). For the experimental procedures involving tissues from human participants, exemption for patient consent was granted by the Biomedical Ethics Review Committee, West China Hospital, Sichuan University. The reason for patient consent being waived were the following: i) The subject may not be exposed to more than minimal risks; ii) the exemption from the subject's informed consent will not adversely affect the subject's rights and interests; iii) the use of identifiable human material or data for research, the subject can no longer be found, and the research project does not involve personal privacy and commercial interests.

Patient consent for publication

Not applicable.

Competing interests

The authors declare that they have no competing interests.

References

1. Llovet JM, Kelley RK, Villanueva A, Singal AG, Pikarsky E, Roayaie S, Lencioni R, Koike K, Zucman-Rossi J and Finn RS: Hepatocellular carcinoma. Nat Rev Dis Primers 7: 6, 2021.
2. McGlynn KA, Petrick JL and El-Serag HB: Epidemiology of hepatocellular carcinoma. Hepatology 73 (Suppl 1): S4-S13, 2021.
3. Llovet JM, Pinyol R, Kelley RK, El-Khoueiry A, Reeves HL, Wang XW, Gores GJ and Villanueva A: Molecular pathogenesis and systemic therapies for hepatocellular carcinoma. Nat Cancer 3: 386-401, 2022.
4. Feng J, Li J, Wu L, Yu Q, Ji J, Wu J, Dai W and Guo C: Emerging roles and the regulation of aerobic glycolysis in hepatocellular carcinoma. J Exp Clin Cancer Res 39: 126, 2020.
5. Du D, Liu C, Qin M, Zhang X, Xi T, Yuan S, Hao H and Xiong J: Metabolic dysregulation and emerging therapeutical targets for hepatocellular carcinoma. Acta Pharm Sin B 12: 558-580, 2022.
6. Zhang Y, Zhai Z, Duan J, Wang X, Zhong J, Wu L, Li A, Cao M, Wu Y, Shi H, *et al*: Lactate: The mediator of metabolism and immunosuppression. Front Endocrinol (Lausanne) 13: 901495, 2022.
7. Zhang QY, Ho DW, Tsui YM and Ng IO: Single-cell transcriptomics of liver cancer: Hype or insights? Cell Mol Gastroenterol Hepatol 14: 513-525, 2022.
8. Aliya S, Lee H, Alhammadi M, Umapathi R and Huh YS: An overview on single-cell technology for hepatocellular carcinoma diagnosis. Int J Mol Sci 23: 1402, 2022.
9. Zhang Y, Wang D, Peng M, Tang L, Ouyang J, Xiong F, Guo C, Tang Y, Zhou Y, Liao Q, *et al*: Single-cell RNA sequencing in cancer research. J Exp Clin Cancer Res 40: 81, 2021.
10. Lei Y, Tang R, Xu J, Wang W, Zhang B, Liu J, Yu X and Shi S: Applications of single-cell sequencing in cancer research: Progress and perspectives. J Hematol Oncol 14: 91, 2021.
11. Martens JH and Stunnenberg HG: BLUEPRINT: Mapping human blood cell epigenomes. Haematologica 98: 1487-1489, 2013.
12. ENCODE Project Consortium: An integrated encyclopedia of DNA elements in the human genome. Nature 489: 57-74, 2012.
13. Mabbott NA, Baillie JK, Brown H, Freeman TC and Hume DA: An expression atlas of human primary cells: Inference of gene function from coexpression networks. BMC Genomics 14: 632, 2013.
14. Schmiedel BJ, Singh D, Madrigal A, Valdovino-Gonzalez AG, White BM, Zapardiel-Gonzalo J, Ha B, Altay G, Greenbaum JA, McVicker G, *et al*: Impact of genetic polymorphisms on human immune cell gene expression. Cell 175: 1701-15.e16, 2018.
15. Livak KJ and Schmittgen TD: Analysis of relative gene expression data using real-time quantitative PCR and the 2(-Delta Delta C(T)) method. Methods 25: 402-408, 2001.
16. Brown ZJ, Tsilimigras DI, Ruff SM, Mohseni A, Kamel IR, Cloyd JM and Pawlik TM: Management of hepatocellular carcinoma: A review. JAMA Surg 158: 410-420, 2023.
17. Wen N, Cai Y, Li F, Ye H, Tang W, Song P and Cheng N: The clinical management of hepatocellular carcinoma worldwide: A concise review and comparison of current guidelines: 2022 Update. Biosci Trends 16: 20-30, 2022.
18. Chidambaranathan-Reghupaty S, Fisher PB and Sarkar D: Hepatocellular carcinoma (HCC): Epidemiology, etiology and molecular classification. Adv Cancer Res 149: 1-61, 2021.
19. Vogel A, Meyer T, Sapisochin G, Salem R and Saborowski A: Hepatocellular carcinoma. Lancet 400: 1345-1362, 2022.
20. Zhang Q, Lou Y, Yang J, Wang J, Feng J, Zhao Y, Wang L, Huang X, Fu Q, Ye M, *et al*: Integrated multiomic analysis reveals comprehensive tumour heterogeneity and novel immunophenotypic classification in hepatocellular carcinomas. Gut 68: 2019-2031, 2019.
21. Sperandio RC, Pestana RC, Miyamura BV and Kaseb AO: Hepatocellular carcinoma immunotherapy. Annu Rev Med 73: 267-278, 2022.
22. Liu Z, Liu X, Liang J, Liu Y, Hou X, Zhang M, Li Y and Jiang X: Immunotherapy for hepatocellular carcinoma: Current status and future prospects. Front Immunol 12: 765101, 2021.
23. Jiang Y, Han QJ and Zhang J: Hepatocellular carcinoma: Mechanisms of progression and immunotherapy. World J Gastroenterol 25: 3151-3167, 2019.
24. Chen L, Huang L, Gu Y, Cang W, Sun P and Xiang Y: Lactate-lactylation hands between metabolic reprogramming and immunosuppression. Int J Mol Sci 23: 11943, 2022.
25. Ganapathy-Kanniappan S: Linking tumor glycolysis and immune evasion in cancer: Emerging concepts and therapeutic opportunities. Biochim Biophys Acta Rev Cancer 1868: 212-220, 2017.
26. Ganapathy-Kanniappan S and Geschwind JF: Tumor glycolysis as a target for cancer therapy: Progress and prospects. Mol Cancer 12: 152, 2013.
27. Su X, Zhao L, Shi Y, Zhang R, Long Q, Bai S, Luo Q, Lin Y, Zou X, Ghazanfar S, *et al*: Clonal evolution in liver cancer at single-cell and single-variant resolution. J Hematol Oncol 14: 22, 2021.
28. Li Y, Song Z, Han Q, Zhao H, Pan Z, Lei Z and Zhang J: Targeted inhibition of STAT3 induces immunogenic cell death of hepatocellular carcinoma cells via glycolysis. Mol Oncol 16: 2861-2880, 2022.
29. Matsumoto K, Noda T, Kobayashi S, Sakano Y, Yokota Y, Iwagami Y, Yamada D, Tomimaru Y, Akita H, Gotoh K, *et al*: Inhibition of glycolytic activator PFKFB3 suppresses tumor growth and induces tumor vessel normalization in hepatocellular carcinoma. Cancer Lett 500: 29-40, 2021.
30. Chen DP, Ning WR, Jiang ZZ, Peng ZP, Zhu LY, Zhuang SM, Kuang DM, Zheng L and Wu Y: Glycolytic activation of peritumoral monocytes fosters immune privilege via the PFKFB3-PD-L1 axis in human hepatocellular carcinoma. J Hepatol 71: 333-343, 2019.
31. Suthen S, Lim CJ, Nguyen PHD, Dutertre CA, Lai HLH, Wasser M, Chua C, Lim TKH, Leow WQ, Loh TJ, *et al*: Hypoxia-driven immunosuppression by Treg and type-2 conventional dendritic cells in HCC. Hepatology 76: 1329-1344, 2022.
32. Lu LG, Zhou ZL, Wang XY, Liu BY, Lu JY, Liu S, Zhang GB, Zhan MX and Chen Y: PD-L1 blockade liberates intrinsic antitumourigenic properties of glycolytic macrophages in hepatocellular carcinoma. Gut 71: 2551-2560, 2022.
33. Cheng K, Cai N, Zhu J, Yang X, Liang H and Zhang W: Tumor-associated macrophages in liver cancer: From mechanisms to therapy. Cancer Commun (Lond) 42: 1112-1140, 2022.
34. Wculek SK, Cueto FJ, Mujal AM, Melero I, Krummel MF and Sancho D: Dendritic cells in cancer immunology and immunotherapy. Nat Rev Immunol 20: 7-24, 2020.
35. Xu F, Jin T, Zhu Y and Dai C: Immune checkpoint therapy in liver cancer. J Exp Clin Cancer Res 37: 110, 2018.
36. Huang CF, Huang CY, Yeh ML, Wang SC, Chen KY, Ko YM, Lin CC, Tsai YS, Tsai PC, Lin ZY, *et al*: Genetics variants and serum levels of MHC class I chain-related A in predicting hepatocellular carcinoma development in chronic hepatitis C patients post antiviral treatment. EBioMedicine 15: 81-89, 2017.
37. Sajid M, Liu L and Sun C: The dynamic role of NK cells in liver cancers: Role in HCC and HBV associated HCC and its therapeutic implications. Front Immunol 13: 887186, 2022.
38. Garnelo M, Tan A, Her Z, Yeong J, Lim CJ, Chen J, Lim KH, Weber A, Chow P, Chung A, *et al*: Interaction between tumour-infiltrating B cells and T cells controls the progression of hepatocellular carcinoma. Gut 66: 342-351, 2017.
39. Dunn GP, Koebel CM and Schreiber RD: Interferons, immunity and cancer immunoediting. Nat Rev Immunol 6: 836-848, 2006.
40. Donne R and Lujambio A: The liver cancer immune microenvironment: Therapeutic implications for hepatocellular carcinoma. Hepatology 77: 1773-1796, 2023.
41. Fu J, Li K, Zhang W, Wan C, Zhang J, Jiang P and Liu XS: Large-scale public data reuse to model immunotherapy response and resistance. Genome Med 12: 21, 2020.
42. Cappellesso F, Orban MP, Shirgaonkar N, Berardi E, Serneels J, Neveu MA, Di Molfetta D, Piccapane F, Caroppo R, Debellis L, *et al*: Targeting the bicarbonate transporter SLC4A4 overcomes immunosuppression and immunotherapy resistance in pancreatic cancer. Nat Cancer 3: 1464-1483, 2022.
43. Ganapathy-Kanniappan S: Taming tumor glycolysis and potential implications for immunotherapy. Front Oncol 7: 36, 2017.
44. Gong Y, Ji P, Yang YS, Xie S, Yu TJ, Xiao Y, Jin ML, Ma D, Guo LW, Pei YC, *et al*: Metabolic-pathway-based subtyping of triple-negative breast cancer reveals potential therapeutic targets. Cell Metab 33: 51-64.e9, 2021.
45. Li X, Han M, Zhang H, Liu F, Pan Y, Zhu J, Liao Z, Chen X and Zhang B: Structures and biological functions of zinc finger proteins and their roles in hepatocellular carcinoma. Biomark Res 10: 2, 2022.

46. Shen Y, Zhang Y, Xiong Y, Zhang Z, Zhang B, Li A, Zhang Z, Ding J, Du J and Che Y: Whole exome sequencing identifies genetic variants in Chinese Han pregnant women with venous thromboembolism. Thromb Res 211: 49-55, 2022.
47. Guo HJ, Wang LJ, Wang C, Guo DZ, Xu BH, Guo XQ and Li H: Identification of an Apis cerana zinc finger protein 41 gene and its involvement in the oxidative stress response. Arch Insect Biochem Physiol 108: e21830, 2021.
48. Jiang P, He S, Li Y and Xu Z: Identification of therapeutic and prognostic biomarkers of Lamin C (LAMC) family members in head and neck squamous cell carcinoma. Med Sci Monit 26: e925735, 2020.
49. Yamada N, Yasui K, Dohi O, Gen Y, Tomie A, Kitaichi T, Iwai N, Mitsuyoshi H, Sumida Y, Moriguchi M, *et al*: Genome-wide DNA methylation analysis in hepatocellular carcinoma. Oncol Rep 35: 2228-2236, 2016.
50. Fu H, Gao H, Qi X, Zhao L, Wu D, Bai Y, Li H, Liu X, Hu J and Shao S: Aldolase A promotes proliferation and G_1/S transition via the EGFR/MAPK pathway in non-small cell lung cancer. Cancer Commun (Lond) 38: 18, 2018.
51. Sun M, Li L, Niu Y, Wang Y, Yan Q, Xie F, Qiao Y, Song J, Sun H, Li Z, *et al*: PRMT6 promotes tumorigenicity and cisplatin response of lung cancer through triggering 6PGD/ENO1 mediated cell metabolism. Acta Pharm Sin B 13: 157-173, 2023.
52. Zhu Y, Jin L, Shi R, Li J, Wang Y, Zhang L, Liang CZ, Narayana VK, De Souza DP, Thorne RF, *et al*: The long noncoding RNA glycoLINC assembles a lower glycolytic metabolon to promote glycolysis. Mol Cell 82: 542-554.e6, 2022.
53. Pan M, Luo M, Liu L, Chen Y, Cheng Z, Wang K, Huang L, Tang N, Qiu J, Huang A and Xia J: EGR1 suppresses HCC growth and aerobic glycolysis by transcriptionally downregulating PFKL. J Exp Clin Cancer Res 43: 35, 2024.
54. Zheng C, Yu X, Liang Y, Zhu Y, He Y, Liao L, Wang D, Yang Y, Yin X, Li A, *et al*: Targeting PFKL with penfluridol inhibits glycolysis and suppresses esophageal cancer tumorigenesis in an AMPK/FOXO3a/BIM-dependent manner. Acta Pharm Sin B 12: 1271-1287, 2022.
55. Bian Z, Yang F, Xu P, Gao G, Yang C, Cao Y, Yao S, Wang X, Yin Y, Fei B and Huang Z: LINC01852 inhibits the tumorigenesis and chemoresistance in colorectal cancer by suppressing SRSF5-mediated alternative splicing of PKM. Mol Cancer 23: 23, 2024.
56. Chen Z, He Q, Lu T, Wu J, Shi G, He L, Zong H, Liu B and Zhu P: mcPGK1-dependent mitochondrial import of PGK1 promotes metabolic reprogramming and self-renewal of liver TICs. Nat Commun 14: 1121, 2023.

Copyright © 2024 Teng et al. This work is licensed under a Creative Commons Attribution-NonCommercial-NoDerivatives 4.0 International (CC BY-NC-ND 4.0) License.